ChemElectroChem

Research Article
doi.org/10.1002/celc.202300270

Chemistry
Europe
European Chemical
Societies Publishing

www.chemelectrochem.org

A Physical Impedance Model of Lithium Intercalation into Graphite Electrodes for a Coin-Cell Assembly

Göktug Yesilbas,[a] Chun-Yu Chou,[a, b] and Aliaksandr S. Bandarenka*[a]

Graphite electrodes are widely used in commercial metal-ion batteries as anodes. Electrochemical impedance spectroscopy serves as one of the primary non-destructive techniques to obtain key information about various batteries during their operation. However, interpretation of the impedance response of graphite electrodes in contact with common organic electrolytes can be complicated. It is especially challenging, particularly when utilizing the 2-electrode configuration that is common in battery research. In this work, we elaborate on a *physical* impedance model capable of accurately describing the impe-

dance spectra of a graphite│electrolyte│metallic Li system in a coin-cell assembly during two initial charge/discharge cycles. We analyze the dependencies of the model parameters for graphite and metallic lithium as a function of the state of charge to verify the model. Additionally, we suggest that the double layer capacitance values obtained during specific intercalation stages could help to determine if the area-normalized values align with the expected range. The data and the procedure necessary for calibration are provided.

Introduction

After Akira Yoshino developed (1985)[1] and Sony commercialized lithium-ion batteries in 1991,[2] these devices rapidly began to appear in all areas of modern life. The demand for lithium-ion batteries is continually rising, particularly for portable devices that such as phones, computers, and fast-growing car technology. Considering environmental factors, it is evident that energy storage devices should contribute to replacing the widespread fossil-based energy sources in many applications.

Following the increase in of lithium-ion battery demand, various chemistries for these devices have been explored. Although Lithium Titanate Oxide (LTO)[3–7] or silicon-based[8–13] materials have been developed as anode materials, graphite is currently the most widely used anode material.[8,14–18] Graphite has a low stable discharge potential profile closely aligned with that of lithium, a commendable specific capacity, and its widespread utilization due to its relatively low cost, easy accessibility, and abundance.[19] However, solely relying on direct current measurements to monitor specific states and processes at the electrode-electrolyte interfaces, such as state of health (SoH), state of charge (SoC), solid electrolyte

interphase (SEI) growth, etc. have several limitations. These measurements cannot determine the electrochemical reactions directly, but they utilize coulomb counting and potential analysis.

Electrochemical impedance spectroscopy (EIS) serves as a valuable research tool for probing the electrode-electrolyte interface.[20–22] EIS is a highly sensitive technique, capable of detecting even the slightest changes within the cell, including variations in charge transfer resistance (R_{CT}) or changes in SEI thickness. However, interpreting the EIS response requires a physical model for comprehensive understanding of battery systems.[23] A suitable physical model considers non-faradaic contributions, reactions at the electrode-electrolyte interface, and interfacial charge and mass transport. Model analysis enables gathering parameter information to see the important mechanisms of the battery cell. This information allows the observer a clearer picture which part or parts of the battery significantly impact battery lifespan or performance. Contrarily, direct current analysis fails in identifying the primary contributors of State of Health (SoH) or Solid Electrolyte Interface (SEI) growth, since it cannot determine variables such as charge transfer resistance (R_{CT}), SEI parameters, double layer capacitance (C_{DL}), or diffusion properties.

In this work, we develop a physical model based on the three-step mechanism.[23–28] This model describes the adsorption/desorption reactions of the lithium ions on a graphite electrode. Moreover, we supported the results of these findings with direct current measurements. Before deciding on the model, we tried various configurations. However, the error rates indicated that interpreting the impedance responses with those models was challenging. Moreover, we believe and as the literature suggests that solely visually inspecting the fit of the electrochemical impedance spectrum not sufficient.[25]

This model explains the impedance response of the cell consisting of graphite, organic electrolyte, and Li counter electrode in a coin cell assembly (as shown in Figure 1). From

[a] G. Yesilbas, C.-Y. Chou, Prof. Dr. A. S. Bandarenka
     Physik-Department ECS
     Technische Universität München
     James-Franck-Straße 1, 85748 Garching (Germany)
     E-mail: bandarenka@ph.tum.de

[b] C.-Y. Chou
     TUM School of Engineering and Design
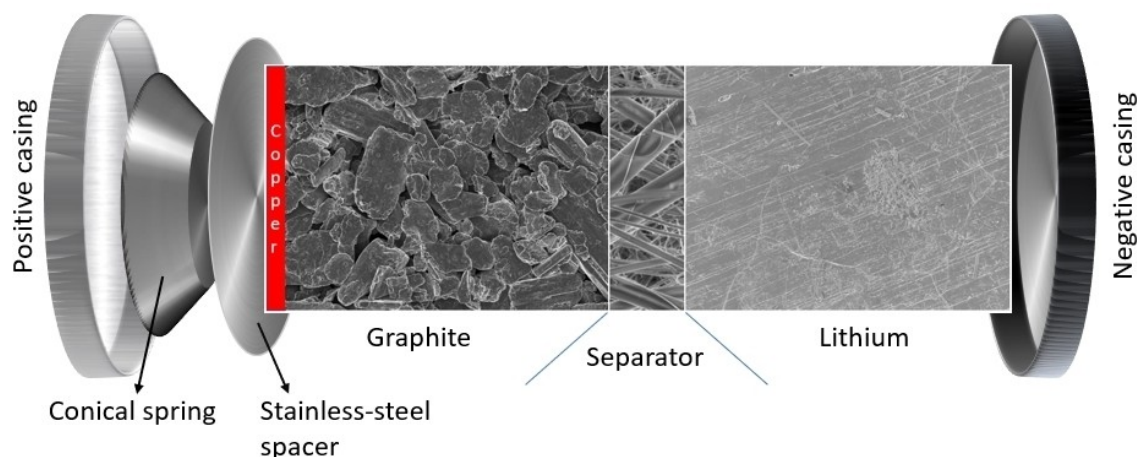   Lichtenbergstraße 4a, 85748 Garching (Germany)

Figure 1. SEM pictures and the internal schematic of the 2-electrode coin cell. From left to right: Positive casing, conical spring, stainless-steel spacer, graphite coated on copper sheet, micro-fiber separator, lithium metal, negative casing.

one perspective, this configuration closely mirrors the standard cell geometry, while Li metal also plays the role of the reference electrode. In other words, the coin cell assembly acts as a standardized configuration, as the cell is convenient for reproducible characterization of graphite electrodes in battery research. Notably, the model separately considers the response of graphite and the response of the Li metal counter/reference electrode. We analyzed the model's parameters as a function of the SoC to ensure its accuracy and validity. In addition, we suggest that the values of the double layer capacitance obtained during the initial stages of intercalation can be used to estimate whether the area-normalized values are within the appropriate range. Necessary calibration data are also provided.

Results And Discussion

Model development

First, we assume that the recent impedance model developed for a flat, highly oriented pyrolytic graphite (HOPG) electrode in contact with a Li^+-containing organic electrolyte[26] is also applicable to the "real-world" graphite powder electrode. At the very surface of graphite, there is a three-stage mechanism of intercalation and deintercalation of Li^+ in the presence of specifically adsorbing/desorbing anions. This mechanism reveals itself under *ac* probing in many intercalation systems[27,28] *via* a specific combination of the following generalized elements $R_{ct,g}$, Z_{G1}, Z_{X1}, Z_{G2}, Z_{X2}, as shown in Figure 2, where $R_{ct,g}$ (Equation 1) is the common charge transfer resistance:
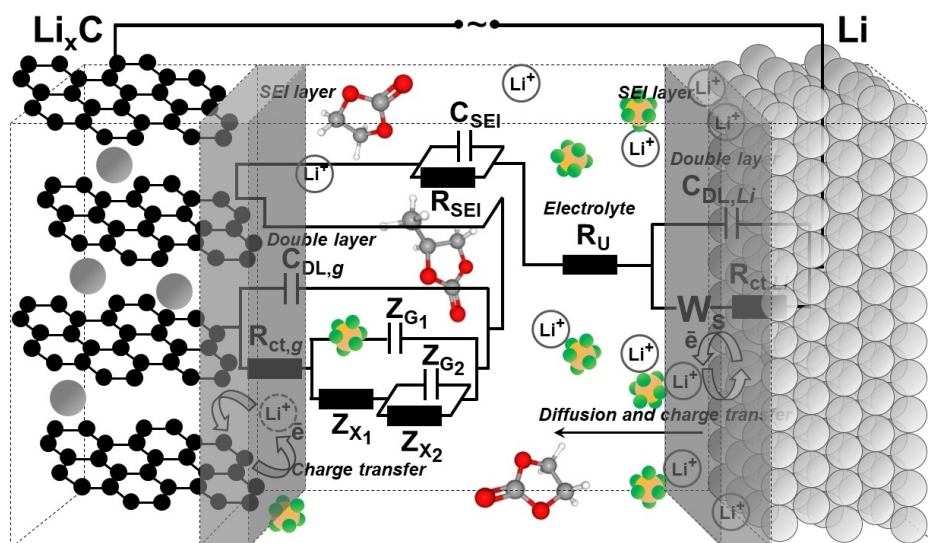
$$R_{ct,g} = (\partial i_{F,g}/\partial E)^{-1}$$

(1)

Figure 2. Equivalent electric circuit of the graphite│electrolyte│metallic Li system in a coin-cell assembly. For the meaning of the elements, see the text.

where $i_{F,g}$ is the Faradaic current at the graphite electrode. The impedances of the other elements are:

$$Z_{G1}, = \pm(j\omega \cdot G1)^{-1};$$
$$Z_{G2}, = \pm(j\omega \cdot G2)^{-1};$$
$$Z_{X1}, = \pm X1;$$
$$Z_{X2}, = \pm X2;$$

(2)

Where j is the imaginary unit, and ω is the angular frequency. The constants G1, G2, X1, and X2 (Equation 2) are formed *via* complex combinations of the kinetic parameters belonging to each of the stages (Li-intercalation/deintercalation, anion adsorption/desorption) of the three-stage mechanism. Specifically on the model, the 1st parallel combination of R–C element represents the simple charge transfer resistance and the double layer capacitance. The subsequent parallel combinations of X–G elements represent the specific adsorption-desorption steps. Importantly, these X–G constants can be positive or negative depending on the electrode potential and relative combinations of the kinetic parameters. In fields like corrosion science, one can potentially use these constants to extract additional information about the electrochemical reaction behavior, but their analysis is not straightforward. In this study, we utilize them to accurately fit the spectra, but we refrain from analyzing their behavior. Further details on the topic can be found in the relevant literature.[26–28] For additional insights on this matter, please check the Supporting Information (Page S8).

Finally, $C_{DL,g}$ is the double layer capacitance of the graphite electrode. Here, one could model the system with a constant-phase element (CPE) instead of $C_{DL,g}$, but the physical interpretation becomes challenging, especially when the dimensionless CPE symmetry exponent drops below 0.8. In our study, the CPE exponent showed values between 0.5 and 0.6, which made the evaluation of the double layer capacitance complex, if not impossible.

Upon the formation of the SEI layer at the surface of the lithium counter electrode and the graphite working electrode, an additional pair of elements C_{SEI} and R_{SEI} (as illustrated in Figure 2) appear, denoting the capacitance and resistance of the SEI, respectively. Normally, expression of the SEI formation demands representation with two R–C parallel circuits, one for reflecting the lithium SEI and the other one for graphite SEI. However, the addition of two R–C parallel circuits brings an empirical challenge, where the computational tools fail to differentiate the specific R–C circuit associated with each electrode. When the secondary R–C circuit is introduced for SEI layer representation, the values for SEI parameters change constantly through each iteration. Consequently, a singular SEI circuit is used for both electrodes. This approach is supported by the SEI capacity calculations. Further details can be found in the Supporting Information (Page S12). If one, for instance, knows the relative permittivity ε_r of the SEI, one can estimate the effective thickness of this layer.[26]

Going further toward the metallic Li-electrode in Figure 2, one can see the electrolyte resistance, R_U, and elements representing the electrified interface between metallic Li and the electrolyte. $C_{DL,Li}$ represents the double layer capacitance of the Li-electrode, while the Faradaic component is represented by the charge transfer resistance $R_{ct,Li}$, and, due to likely very high-speed lithium reduction/oxidation, finite length diffusion Warburg (short) element (Equation 3) with the impedance given as:

$$Z_{Ws}(\omega) = W_s r(\omega)^{-0.5}(1-j)\tanh[W_s c(j\omega)^{0.5}] \quad (3)$$

Warburg short element has two parameters which are $W_s r$, the Warburg coefficient ($\Omega/s^{1/2}$), and $W_s c$ ($s^{1/2}$), which is the parameter (Equation 4) proportional to the Nernst diffusion layer thickness:[29–32]

$$W_s c = d/D^{0.5} \quad (4)$$

where d is the Nernst diffusion layer thickness and D is the diffusion coefficient.

Model verification

The represented mechanism comprises three stages, assuming that each process at the interface (which involves the electrolyte component's adsorption-desorption) is reversible. To verify this reversibility, we conducted a cyclic voltammetry experiment on the graphite electrode. Figure 3 represents the cyclic voltammetry curves of the graphite electrode in 1 M LiPF$_6$ in EC:DEC (1:1) with a 1 mV s^{-1} scan rate. From the cyclic voltammogram, it is evident the electrochemical process is largely reversible.

Figure 4 presents the potential profile of the graphite electrode for the first lithiation-delithiation cycle. The three plateaus (stages)[8,15,17,33,34] are clearly visible in the figure. Notably, the SEI formation dominantly occurs between 0.8 V and 0.6 V vs. Li/Li$^+$ during the first lithiation cycle. However, it is important to point out that the SEI continues to grow throughout each cycle. Therefore, the experiment specifically targets varying potentials during the initial cycle, with chosen potentials represented by black dots in Figure 4. The SEI is composed of organic and inorganic fragments (see Table S2 in Supporting Information). SEI also acts as a "filter" for the battery and allows lithium-ion transport, meanwhile stopping the electrons and bigger molecules that should not intercalate into the graphite layers.[16,35,36]

Figure 5A shows a typical impedance spectrum obtained during first lithiation cycle. A similar impedance behavior was also reported in the literature by Shoutau Li et al. (2020) even after 800 cycles.[37] One can clearly distinguish typical features at different frequencies, which likely correspond to the formation of the SEI, Faradaic processes at the graphite and Li-metal electrodes, and diffusion of Li$^+$ into and out of Li-metal electrodes. It is worth mentioning that Faradaic processes at the counter electrodes should demonstrate local fast kinetics. Interestingly, the model presented in Figure 2 can describe the spectrum with root-mean-squared deviations of less than 2.5%
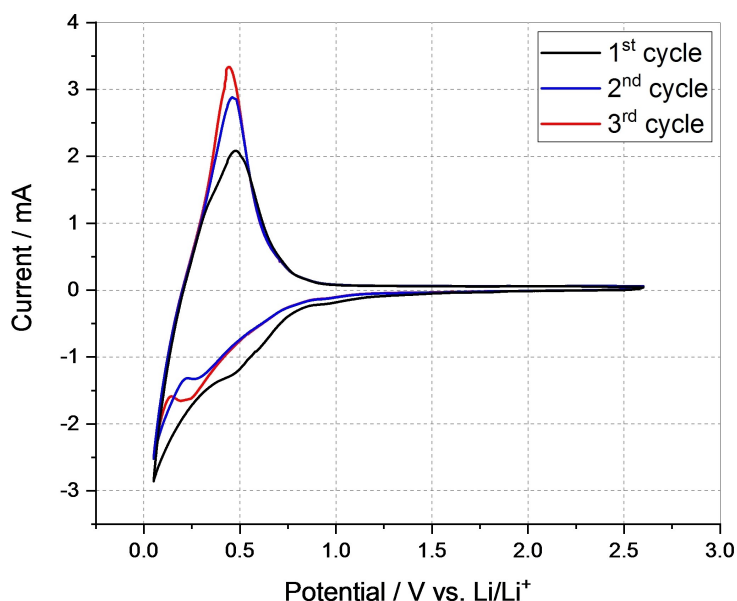
Figure 3. Cyclic voltammetry curves of the graphite electrode in 1 M LiPF$_6$ in EC:DEC (1:1), scan rate: 1 mVs^{-1}.
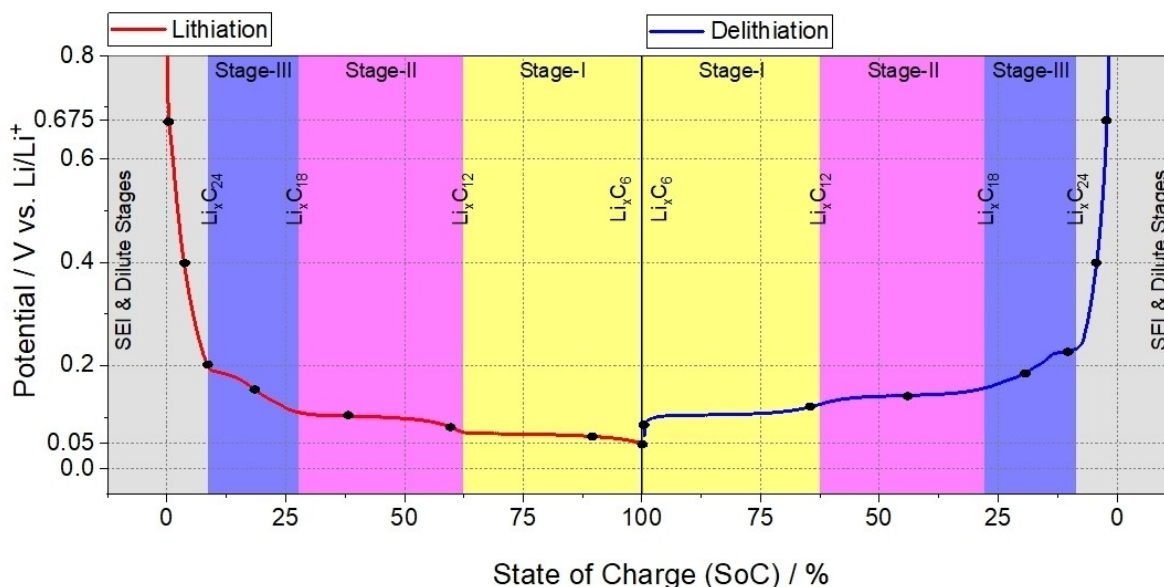

Figure 4. Potential profile and the chosen experimental potential points of the first cycle for PEIS measurements of the Graphite electrode in 1 M LiPF$_6$ in EC:DEC (1:1, volume:volume) at 25°C.

error rate in the whole frequency range with relatively small estimated individual parameter errors. This suggests that every element in the model contributes to the description of the overall response.[38,39] Moreover, this model demonstrates good fitting results for all the points selected for the measurements. The complete two cycles of lithiation and delithiation fitting results using presented model for different SoC are shown in Figure 5B,C,D,E. The low-frequency diffusion part changes drastically after the first cycle, and it is essential to note that these deviations can be caused by porosity impedance.[40–42]

It is now essential to follow and verify the parameters of the model as a function of the SoC. We have presented a complete set of parameters alongside additional materials, and these have been compared to T-311 in Table S3, Table S4 and Table S5 of the Supporting Information. Below, we discuss the most important parameters in more detail. Figure 6 presents the parameters R$_{SEI}$ and C$_{SEI}$, which are associated to the formation of the SEI layer as a function of SoC during the initial two lithiation-delithiation cycles.

As shown in Figure 6A, the resistance of the film significantly drops during the first lithiation cycle and then decreases further in the subsequent cycle. Such behavior is rather expected since the film's conductivity usually stabilizes after 2–3 cycles (2–3 SEI formation cycles performed for the commercial
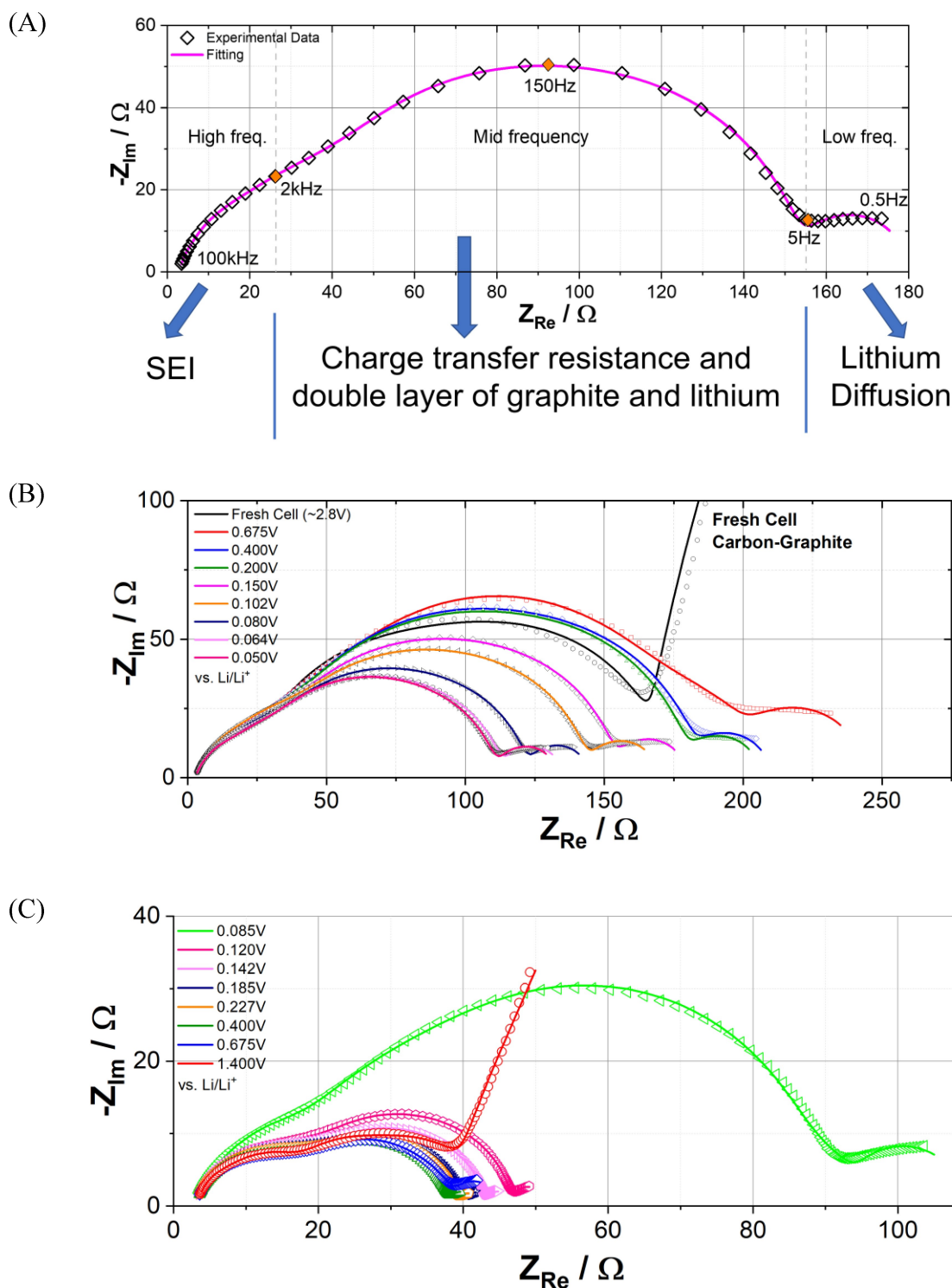
Figure 5. (A) Nyquist plot of a typical impedance spectrum of the graphite electrode recorded at 0.150 V at 25 °C in the first lithiation cycle with the highlighted frequency ranges (solid line represents the fitting to the model shown in Figure 2). Nyquist plots and the fittings of the impedance spectrum of the (B) first lithiation cycle, (C) first delithiation cycle, (D) second lithiaton cycle, and (E) second delithiation cycle of the graphite electrode in 1 M LiPF$_6$ in EC:DEC (1:1, v:v) at 25 °C from the fresh cell (~2.8 V) to 0.050 V. Charging rate: C/20.

cells as a part of the manufacturing procedure) as a result of "self-doping".[43,44] In the first cycle, the values of the C$_{SEI}$ are relatively high, ranging from ~2 to ~8 μF/cm^2. However, in the second lithiation cycle, as the film thickens, this parameter predictably decreases to ~1 μF/cm^2 and sees only minor changes thereafter. Additional details can be found in the Supporting Information (Page S14).

ChemElectroChem

Research Article
doi.org/10.1002/celc.202300270

Chemistry Europe
European Chemical
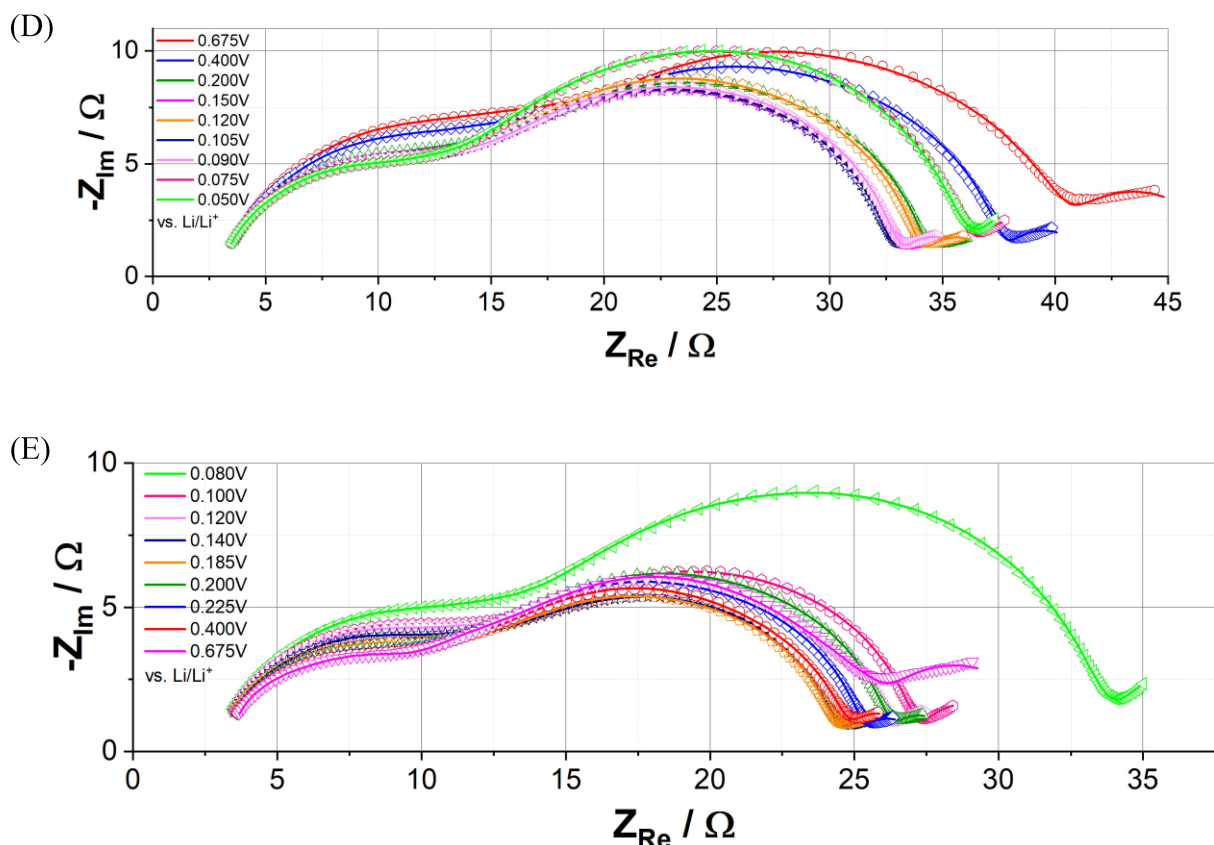Societies Publishing

(D)

(E)

Figure 7 presents the normalized double layer capacitance variations for the graphite electrodes. During electrode cycling, there is a tendency to increase the double layer capacitance values. It is essential to point out that this could result from the formation of the SEI film in the first cycle, which is likely to primarily affect the diffuse part of the double layer. This value is dependent on the composition of the electrolyte, additives, and even the film layer's homogeneity. The contribution of the compact part becomes even more significant in the second cycle, leading to an effective increase of the measured $C_{DL,g}$.

What is remarkable in the dependence shown in Figure 7A is that the values remain nearly constant in the electrode potential range of ~0.1 V to ~1.4 V during the first delithiation cycle, showing approximately 0.93 μF/cm2 of carbon graphite electrode. In the second lithiation cycle, the values remain almost constant between ~0.675 V and ~0.05 V, with capacitances of about 1.5 μF/cm^2.

Together with these values of the double layer capacitance, one can, in principle, non-destructively assess whether the area-normalized values are within the appropriate range or not.

The charge transfer resistance tends to decrease in the first cycle, stabilizing at approximately 3 Ω cm^2 in the second lithiation-delithiation loop, as shown in Figure 7B.
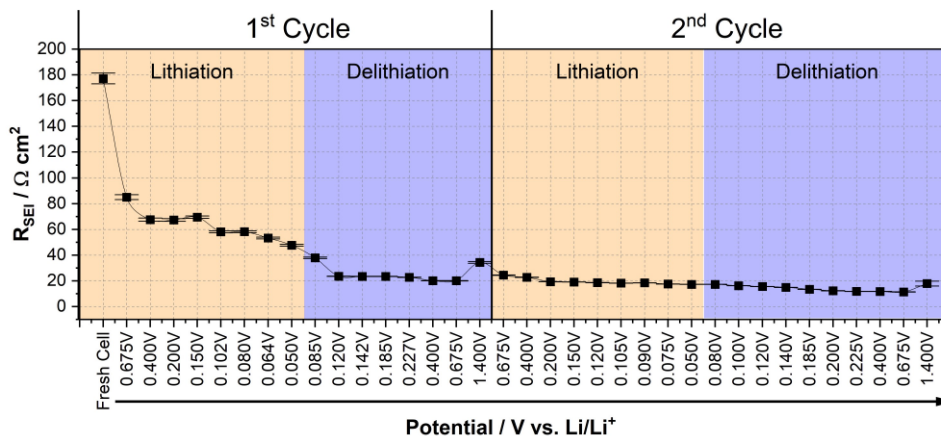
Finally, Figure 8 represents the variations in the parameters of the impedance model attributed to the Li-metal electrode. It is important to note that the potentials in the figure are provided for the graphite electrode *vs.* Li$^+$/Li to give an idea about the SoC of the graphite working electrode during cycling.

This approach allows us to compare the same system states for both electrodes. The double layer capacitances (see Figure 8A) of the metallic Li-electrode are quite large, which is typical for metal electrodes, and they vary significantly depending on the cycle stage. Another significant observation is the sharp increases during the lithiation of the metallic lithium counter electrode. Such process could lead to dendrite formation on the lithium surface,[45,46] consequently increasing the surface area. For more insight, please refer to the Supporting Information (Page S5). Although 3-electrode measurements also show similar characteristics, directly assessing the double layer capacitance of the lithium is not trivial due to the SEI formation on the lithium metal and its reactivity. The dynamics of the charge transfer resistance (as shown in Figure 8B) for the reduction/oxidation of lithium is similar to that of the graphite electrode. It generally decreases with cycling, and it shows stabilizing characteristics in the second cycle.

Warburg short (W_s) represents the Li diffusion at the lithium metal counter electrode. Moreover, the diffusional impedance is mostly dominated by the counter electrode (refer to the Supporting Information (Figure S16)). The parameter of the Warburg impedance, W_sc, can be used to estimate the Nernst diffusion layer thickness as detailed in Equation 4. To further elaborate on the validity of the proposed impedance model, the values of the diffusion coefficient of Li$^+$ in the electrolyte are required.

Capigilia et al. in 1999[47] reported that the diffusion coefficient of the Li$^+$ ions in ethylene carbonate:ethyl methyl

ChemElectroChem

Research Article
doi.org/10.1002/celc.202300270

**Chemistry
Europe**

European Chemical
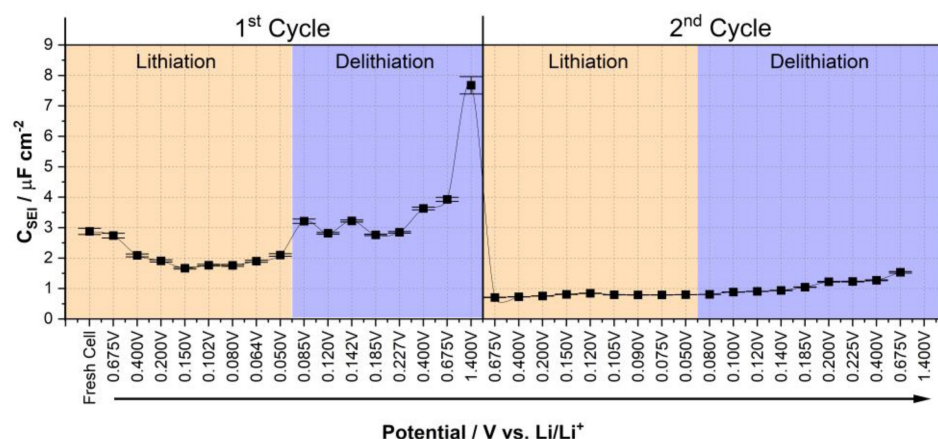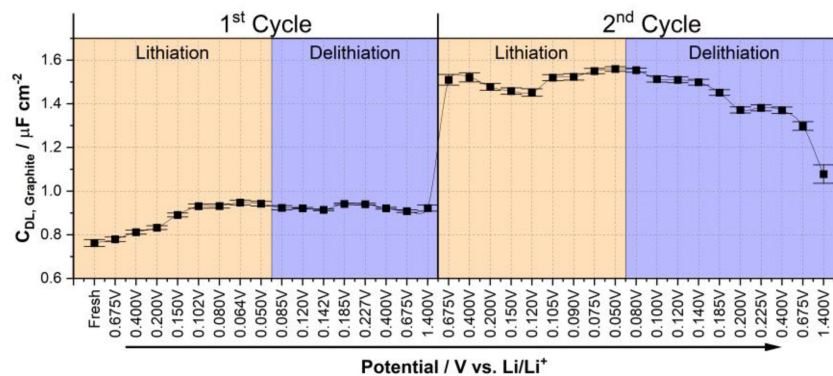Societies Publishing

(A)

(B)

Figure 6. Dependencies of the parameters associated with the formation of the SEI obtained during lithiation and delithiation for two cycles. (A) Resistance and (B) capacitance of the SEI film.

carbonate (EC:EMC) changed from 4.5×10^{-6} cm^2/s to 5×10^{-6} cm^2/s for 1 M LiPF$_6$. In a subsequent study in 2000, Capiglia et al.[48] showed that the diffusion coefficient of the Li$^+$ ions varied from 1.53×10^{-6} cm^2/s to 6.07×10^{-7} cm^2/s in EC:DEC. Valøen and Reimers in 2005[49] reported that the diffusion coefficient of the Li$^+$ ions for 1 M solutions at 294 °K ranged from 3×10^{-6} cm^2/s to 4×10^{-6} cm^2/s in propylene carbonate:ethylene carbonate:ethyl methyl carbonate (PC:EC:EMC). K. Hayamizu in 2012[50] reported the diffusion coefficient of the Li$^+$ ions for 1 M solutions at 293° K to be between 0.952×10^{-6} cm^2/s and 1.47×10^{-6} cm^2/s in different mixture ratios of EC:DEC. J. Landesfeind and H. A. Gasteiger in 2019[51] reported that the diffusion coefficient of the Li$^+$ ions to be around 3×10^{-6} cm^2/s at 20 °C for 1 M LiPF$_6$ in ethylene carbonate:dimethyl carbonate (EC:DMC). J. Landesfeind et al. in 2021[52] showed that the diffusion coefficient of Li$^+$ ions to be approximately 2.5×10^{-6} cm^2/s at 25°. C. H. Lundren et al. in 2014[53] presented the diffusion coefficient of Li$^+$ ions to be around 2.5×10^{-6} cm^2/s at 25 °C. As illustrated by the data, the diffusion coefficient of

the lithium ions is approximately 3×10^{-6} cm^2/s ($\pm 1 \times 10^{-6}$ cm^2/s). By using this information, the Nernst diffusion layer thickness calculation[54] values are presented in Figure 8C. As observed from the figure, values for the Nernst diffusion layer thickness vary around 10 μm, which is typical for liquid electrolyte electrochemical systems, additionally confirming the validity of the developed model.

Moreover, it was considered to add the second Warburg element to represent the lithium diffusion on the working electrode. However, considering the impedance contribution of the electrodes, only representing the lithium side is more logical due to the complexity of the modeling with two Warburg elements, which are often indistinguishable by the impedance fitting tools. Using two Warburg elements makes the interpretation extremely complicated, and the particular element error values increase to three digits or even higher. For additional details, including the results of the experiments using different graphite powders, please check the Supporting Information, Page S17.

ChemElectroChem

Research Article
doi.org/10.1002/celc.202300270

Chemistry
Europe

European Chemical
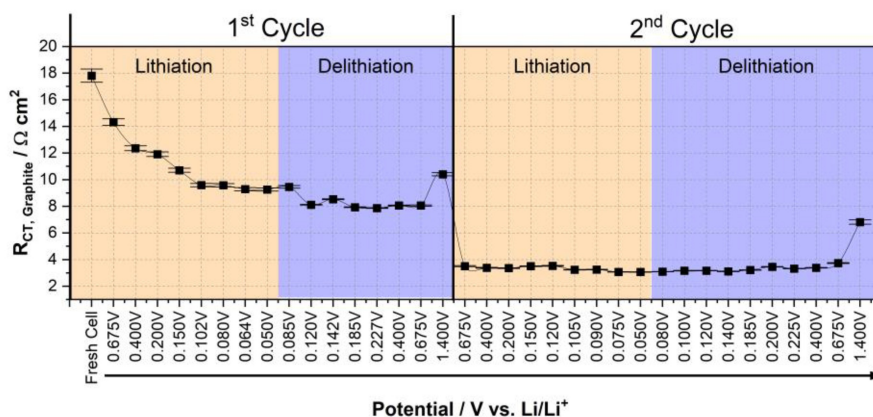Societies Publishing

(A)

(B)

Figure 7. (A) The double layer capacitance of the graphite electrode and (B) the charge transfer resistance at the graphite surface as a function of the cell potential in two lithiation-delithiation cycles.

Conclusions

In conclusion, our proposed physical model offers a detailed analysis of impedance measurements for a 2-electrode system (graphite | electrolyte | metallic Li) during the initial stages of the lithium intercalation into the graphite electrode. By sequentially lithiating and delithiating the graphite electrode at specific intercalation-stage potentials over two cycles, we effectively validated this model. This approach allowed us to gather information about different cell parameters from the impedance spectra fittings. These parameters include the double layer capacitance, charge transfer resistance, and even the diffusion parameters related with the Li-electrode. Moreover, the model offers a comprehensive characterization of SEI formation for both the counter electrode and the working electrode, particularly when supported with 3-electrode impedance measurements. A key finding from our analysis is the presence of mass transport limitations from the Li-electrode side. This finding enabled us to determine the Nernst diffusion layer thickness, which is approximately 10 μm. Additionally, our model is capable of modeling other graphite materials with comparable double layer capacitance and charge transfer resistance values. This assessment is supported with three
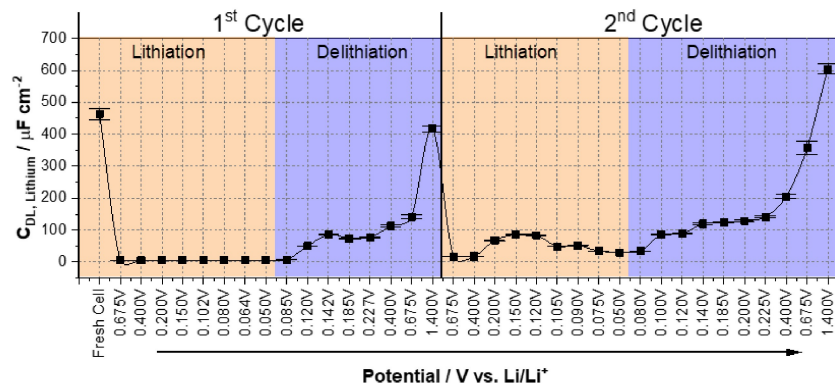
different graphite powders. Lastly, we believe that the specific double layer capacitance values of the graphite electrode, obtained at certain intercalation stages, could serve as a benchmark. These values could help to determine whether the area-normalized values align within an expected and meaningful range.
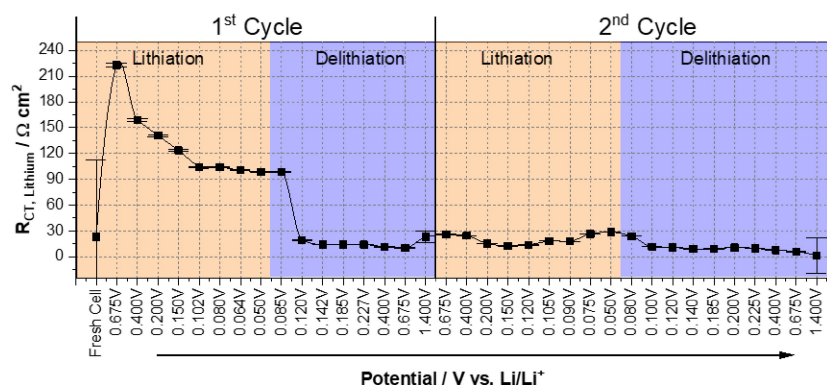
Supporting Information

Supporting Information contains the test procedure of the 2-electrode setup and provides background of three-stage mechanism for Li-ion batteries. Additionally, it offers details about the fitting procedure and insights of the 3-electrode coin cell setup. A comparison between the 3- and 2-electrode parameters is also represented. The superiority of a 2-electrode coin cell setup over a 3-electrode coin cell setup is also explained. Furthermore, impedance parameters and their analyses for two additional graphite powders are included.

The authors have cited additional references within the Supporting Information.[55–59]

ChemElectroChem

Research Article
doi.org/10.1002/celc.202300270

**Chemistry
Europe**
European Chemical
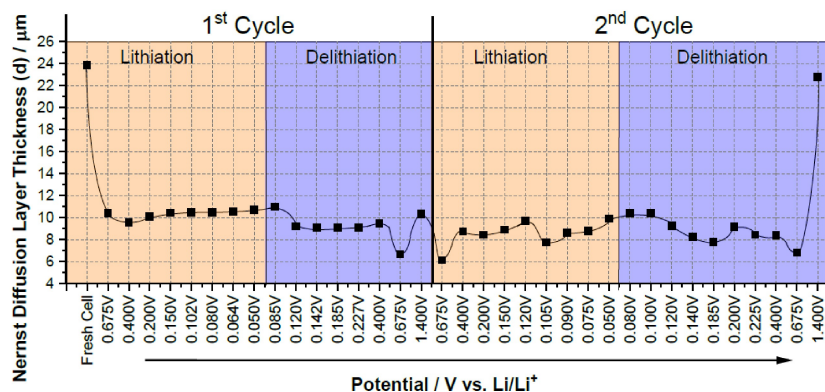Societies Publishing

(A)

(B)

(C)

Figure 8. Variations of the parameters related to the Li-metal electrode depending on the state of charge of the graphite electrode: (A) the double layer capacitance, (B) the charge transfer resistance and (C) the Nernst diffusion layer thickness calculated based on the diffusional Warburg impedance. Note that the potentials in this figure are given for the graphite electrode vs Li$^+$/Li.

Experimental

Graphite electrode preparation

The graphite electrode was prepared by mixing 95% finely grounded graphite powder (T-311, SGL Carbon GMBH) and 5% polyvinylidene difluoride powder (PVDF, Kynar®) as a binder. Subsequently, N-methyl pyrrolidone (NMP, anhydrous, Merck, Germany) was added to the powder mixture with a mass ratio of 5:4 (solid:liquid). This blend was then mixed using a planetary mixer (Thinky Corp., USA) for 15 minutes. The resulting graphite slurry was spread onto a clean battery-grade copper foil (Cu-foil, MTI corp., USA) using a doctor blade mounted gap bar coater (RK Print Coat Instruments, UK). The coated sheet was then dried in an oven at 50°C for at least 3 hours. After drying, the sheets underwent calen3dering to achieve 40% porosity, using a calendaring

ChemElectroChem

Research Article
doi.org/10.1002/celc.202300270

**Chemistry
Europe**
European Chemical
Societies Publishing

machine (GK 300 L, Saueressig GMBH) between two polished stainless-steel cylinders. Then, the processed sheets were punched into 12 mm diameter electrodes using a precision electrode puncher (Aotelec, China). These electrodes were further dried overnight at 120 °C in a dynamic vacuum oven to minimize the residual moisture. Finally, the electrodes were transferred without exposing them to the ambient air to the glovebox (GS MEGA, Glovebox Systemtechnik GMBH, Germany) for the assembly.

Coin-Cell Assembly

The entire the assembly process took place within a glovebox, filled with argon (5.0, 99.999% purity) atmosphere, maintaining levels below 0.3 ppm for both H_2O and O_2. Initially, a circular lithium chip (d: ~16 mm, Mateck, Germany) was cut. The lithium chip's surface was subsequently scratched on both sides using surgical blade to remove contamination and any potentially oxidized layers. This lithium chip was then placed into the negative casing. Following this a glass microfiber separator with a thickness of 175 μm (d: 16 mm, VWR, filter size: 1.6 μm), was positioned. Afterwards, the graphite electrode was placed onto the separator. The separator was then soaked with 120 μl of 1 M $LiPF_6$ (Lithium Hexafluorophosphate) in EC:DEC (Ethylene Carbonate:Diethyl Carbonate 1:1, v:v) battery grade electrolyte (Sigma Aldrich, Germany). Then, a stainless-steel spacer was positioned over the graphite electrode to keep it in place. Prior to sealing the cell, a conical spring was placed between the spacer and the positive casing to ensure pressure and integrity between the electrodes. The final step involved crimping the completed cell with a hydraulic crimping machine (Aotelec, China). All stainless-steel coin cell parts were bought from Aotelec (AOT) Battery Technology Co. (China). Figure 1 schematically shows the resulting assembly using corresponding SEM pictures for each part. For more details on the typical test procedure, please refer to the Supporting Information (Page S1).

Conflict of Interests

The authors declare no conflict of interest.

Data Availability Statement

The data that support the findings of this study are available from the corresponding author upon reasonable request.

Keywords: Anodes · Equivalent circuit · Impedance Spectroscopy · Li-ion batteries · Solid Electrolyte Interface

[1] A. Yoshino, K. Sanechika, T. Nakajima, *US Patent Office* **1987**, US4668595A.
[2] T. Nagaura, K. Tozawa, *JEC Press* **1990**, *9*, p. 209.
[3] F. Ronci, P. Reale, B. Scrosati, S. Panero, V. Rossi Albertini, P. Perfetti, M. di Michiel, J. M. Merino, *J. Phys. Chem. B* **2002**, *106*, 3082–3086.
[4] A. S. Prakash, P. Manikandan, K. Ramesha, M. Sathiya, J.-M. Tarascon, A. K. Shukla, *Chem. Mater.* **2010**, *22*, 2857–2863.
[5] I. Belharouak, G. M. Koenig Jr, K. Amine, *J. Power Sources* **2011**, *196*, 10344–10350.
[6] N. Takami, H. Inagaki, Y. Tatebayashi, H. Saruwatari, K. Honda, S. Egusa, *J. Power Sources* **2013**, *244*, 469–475.
[7] H. Zhang, Y. Yang, H. Xu, L. Wang, X. Lu, X. He, *InfoMat.* **2022**, *4*, e12228.
[8] J. Asenbauer, T. Eisenmann, M. Kuenzel, A. Kazzazi, Z. Chen, D. Bresser, *Sustain. Energy Fuels* **2020**, *4*, 5387–5416.
[9] M. Green, E. Fielder, B. Scrosati, M. Wachtler, J. S. Moreno, *Electrochem. Solid-State Lett.* **2003**, *6*, A75–A79.
[10] H. Jung, M. Park, Y.-G. Yoon, G.-B. Kim, S.-K. Joo, *J. Power Sources* **2003**, *115*, 346–351.
[11] C. K. Chan, H. Peng, G. Liu, K. McIlwrath, X. F. Zhang, R. A. Huggins, Y. Cui, *Nat. Nanotechnol.* **2008**, *3*, 31–35.
[12] A. F. Gonzalez, N.-H. Yang, R.-S. Liu, *J. Phys. Chem. C* **2017**, *121*, 27775–27787.
[13] K. Pan, F. Zou, M. Canova, Y. Zhu, J.-H. Kim, *J. Power Sources* **2020**, *479*, 229083.
[14] Y. Li, Y. Lu, P. Adelhelm, M.-M. Titirici, Y.-S. Hu, *Chem. Soc. Rev.* **2019**, *48*, 4655–4687.
[15] D. Billaud, F. X. Henry, *Solid State Commun.* **2002**, *124*, 299–304.
[16] S. J. An, J. Li, C. Daniel, D. Mohanty, S. Nagpure, D. L. Wood III, *Carbon* **2016**, *105*, 52–76.
[17] Q. Liu, S. Li, S. Wang, X. Zhang, S. Zhou, Y. Bai, J. Zheng, X. Lu, *J. Phys. Chem. Lett.* **2018**, *9*, 5567–5573.
[18] K. Yang, L. Jia, X. Liu, Z. Wang, Y. Wang, Y. Li, H. Chen, B. Wu, L. Yang, F. Pan, *Nano Res.* **2020**, *13*, 412–418.
[19] US Geological Survay Mineral Commodity Summaries. https://pubs.usgs.gov/periodicals/mcs2022/mcs2022-zeolites.pdf (accessed October 10, 2022).
[20] M. Gaberšček, *Nat. Commun.* **2021**, *12*, 6513.
[21] N. Meddings, M. Heinrich, F. Overney, J.-S. Lee, V. Ruiz, E. Napolitano, S. Seitz, G. Hinds, R. Raccichini, M. Gaberšček, J. Park, *J. Power Sources* **2020**, *480*, 228742.
[22] B. Liebhart, M. Satzke, L. Komsiyska, C. Endisch, *J. Power Sources* **2020**, *480*, 228673.
[23] R. R. Gaddam, L. Katzenmeier, X. Lamprecht, A. S. Bandarenka, *Phys. Chem. Chem. Phys.* **2021**, *23*, 12926–12944.
[24] X. Lamprecht, P. Marzak, A. Wieczorek, N. Thomsen, J. Kim, B. Garlyyev, Y. Liang, A. S. Bandarenka, J. Yun, *Energy Adv.* **2022**, *9*, 623–631.
[25] M. G. S. R. Thomas, P. G. Bruce, J. B. Goodenough, *J. Electrochem. Soc.* **1985**, *132*, 1521.
[26] F. Dinkelacker, P. Marzak, J. Yun, Y. Liang, A. S. Bandarenka, *ACS Appl. Mater. Interfaces* **2018**, *10*, 14063–14069.
[27] E. Ventosa, B. Paulitsch, P. Marzak, J. Yun, F. Schiegg, T. Quast, A. S. Bandarenka, *Adv. Sci.* **2016**, *3*, 1600211.
[28] J. Yun, J. Pfisterer, A. S. Bandarenka, *Energy Environ. Sci.* **2016**, *9*, 955–961.
[29] A. Lasia, *Electrochemical Impedance Spectroscopy and its Applications.* Springer **2014**.
[30] B. A. Boukamp, *Equivalent Circuit Users Manual*, University of Twente **1989**.
[31] T. Jacobsen, K. West, *Electrochim. Acta* **1995**, *40*, 255–262.
[32] B. B. Berkes, J. B. Henry, M. Huang, A. S. Bondarenko, *ChemPhysChem* **2012**, *13*, 3210–3217.
[33] A. Shellikeri, V. Watson, D. Adams, E. Kalu, J. Read, J. Jow, J. S. Zheng, J. P. Zheng, *J. Electrochem. Soc.* **2017**, *164*, A3914–A3924.
[34] D. Allart, M. Montaru, H. Gualous, *J. Electrochem. Soc.* **2018**, *165*, A380–A387.
[35] S. H. Beheshti, M. Javanbakht, H. Omidvar, M. S. Hosen, A. Hubin, J. V. Mierlo, M. Berecibar, *iScience* **2022**, *25*, 103862, doi: 10.1016/j.isci.2022.103862.
[36] S. K. Heiskanen, J. Kim, B. L. Lucht, *Joule* **2019**, *3*, 2322–2333.
[37] S. Li, Q. Meng, M. Fan, K. Yang, G. Tian, *Ionics* **2020**, *26*, 4443–4454.
[38] A. S. Bondarenko, *Anal. Chim. Acta* **2012**, *743*, 41.

[39] A. S. Bondarenko, G. A. Ragoisha, *Progress in Chemometrics Research*, ed. A. L. Pomerantsev, Nova Science Publishers, Inc. **2005**, pp. 89–102.

[40] H. D. Yoo, J. H. Jang, J. H. Ryu, Y. Park, S. M. Oh, *J. Power Sources* **2014**, *267*, 411–420.

[41] H. Keiser, K. D. Beccu, M. A. Gutjahr, *Electrochim. Acta* **1976**, *21*, 539–543.

[42] A. Lasia, *J. Electroanal. Chem.* **1995**, *397*, 27–33.

[43] Y. Li, K. Leung, Y. Qi, *Acc. Chem. Res.* **2016**, *49*, 2363–2370.

[44] A. Wang, S. Kadam, H. Li, S. Shi, Y. Qi, *NPJ Comput. Mater.* **2018**, *4*, 15.

[45] Y. Liu, Q. Liu, L. Xin, Y. Liu, F. Yang, E. A. Stach, J. Xie, *Nat. Energy* **2017**, *2*, 17083.

[46] R. Pathak, K. Chen, A. Gurung, K. M. Reza, B. Bahrami, J. Pokharel, A. Baniya, W. He, F. Wu, Y. Zhou, K. Xu, Q. Qiao, *Nat. Commun.* **2020**, *11*, 93.

[47] C. Capiglia, Y. Saito, H. Kageyama, P. Mustarelli, T. Iwamoto, T. Tabuchi, H. Tukamoto, *J. Power Sources* **1999**, *81–82*, 859–862.

[48] C. Capiglia, Y. Saito, H. Yamamoto, H. Kageyama, P. Mustarelli, *Electrochim. Acta* **2000**, *45*, 1341–1345.

[49] L. O. Valøoen, J. N. Reimers, *J. Electrochem. Soc.* **2005**, *152*, A882.

[50] K. Hayamizu, *J. Chem. Eng. Data* **2012**, *57*, 2012–2017.

[51] J. Landesfeind, H. A. Gasteiger, *J. Electrochem. Soc.* **2019**, *166*, A3079–A3097.

[52] J. Landesfeind, T. Hosaka, M. Graf, K. Kubota, S. Komaba, H. A. Gasteiger, *J. Electrochem. Soc.* **2021**, *168*, 040538.

[53] H. Lundgren, M. Behm, G. Lindbergh, *J. Electrochem. Soc.* **2014**, *162*, A413–A420.

[54] M. E. Orazem, B. Tribollet, *Electrochemical Impedance Spectroscopy.* Wiley-Interscience, New York **2008**.

[55] G. J. Brug, A. L. G. van den Eeden, M. Sluyters-Rehbach, J. H. Sluyters, *J. Electroanal. Chem. Interfacial Electrochem.* **1984**, *176*, 275–295.

[56] V. M.-W. Huang, V. Vivier, M. E. Orazem, N. Pébère, B. Tribollet, *J. Electrochem. Soc.* **2007**, *154*, C99.

[57] J.-B. Jorcin, M. E. Orazem, N. Pébère, B. Tribollet, *Electrochim. Acta* **2006**, *51*, 1473–1479.

[58] B. Tribollet, B. Hirschorn, M. E. Orazem, I. Frateur, V. Vivier, *ECS Meet. Abstr.* **2009**, *2*, 3163.

[59] C. Sole, N. E. Drewett, F. Liu, A. M. Abdelkader, I. A. Kinloch, L. J. Hardwick, *J. Electroanal. Chem.* **2015**, *753*, 35–41.